Supporting Information

Adsorption-Induced Deformation of Hierarchically Structured Mesoporous Silica - Effect of Pore-Level Anisotropy

Christian Balzer[†*], Anna M. Waag[†], Stefan Gehret[†], Gudrun Reichenauer[†*], Florian Putz[‡], Nicola Hüsing[‡], Oskar Paris[§], Noam Bernstein[¶], Gennady Y. Gor[⊥*], Alexander V. Neimark[‖*]

[†] Bavarian Center for Applied Energy Research, Magdalene-Schoch-Str. 3, 97074, Wuerzburg, Germany

[‡] Materials Chemistry, Paris Lodron University Salzburg, Jakob-Haringer Str. 2a, 5020 Salzburg, Austria

[§] Institute of Physics, Montanuniversitaet Leoben, Franz-Josef-Str. 18, 8700 Leoben, Austria

[¶] Center for Materials Physics and Technology, U.S. Naval Research Laboratory, Washington, DC 20375, USA

[⊥] Otto H. York Department of Chemical, Biological, and Pharmaceutical Engineering, New Jersey Institute of Technology, University Heights, Newark, NJ 07102, USA

[‖] Rutgers, The State University of New Jersey University, Department of Chemical and Biochemical Engineering, 98 Brett Road, Piscataway, NJ 08854, United States

* Corresponding authors: CB: christian.balzer@zae-bayern.de, GR: gudrun.reichenauer@zae-bayern.de, GYG: gor@njit.edu, AVN: aneimark@rutgers.edu

Derivation of the Frumkin-Derjaguin equation for cylindrical pores

To derive the Frumkin-Derjaguin equation for a cylindrical pore of radius R, length L, surface area $2\pi RL$ and pore volume $V_p = \pi R^2 L$ we consider the free energy of the adsorbate filled pore at saturation. According to Gibbs adsorption equation [1] we get:

$$2\pi RL \cdot \gamma_s - \int_{-\infty}^{0} N_a d\mu = 2\pi RL \cdot \gamma_{sl} \quad (S1)$$

Here γ_s is the surface energy of the solid surface in vacuum and γ_{sl} is the surface energy of the solid surface in contact with liquid. Using Eq. 6 and Eq. 9a we may write

$$\int_{-\infty}^{0} N_a d\mu = [N_a \cdot \mu]_{dry}^{wet} - \int_{0}^{V_p/V_L} \mu dN_a = -\int_{0}^{R} \mu \cdot \frac{dN_a}{dh} dh = 2\pi L \int_{0}^{R} \left[\Pi(h) + \frac{\gamma_{lv}}{R-h}\right] \cdot (R-h) dh$$
$$= 2\pi L \int_{0}^{R} (R-h)\Pi(h) dh + 2\pi RL \cdot \gamma_{lv} \quad (S2)$$

The second equality in Eq. S2 follows from $[N_a \cdot \mu]_{dry}^{wet} = 0$, since $N_a(dry) = 0$ and $\mu(wet) = 0$.

Combining Eq. S1 and S2 results in the Frumkin-Derjaguin equation for the cylindrical pore:

$$\gamma_s = \gamma_{sl} + \gamma_{lv} + \frac{1}{R}\int_{0}^{R} (R-h)\Pi(h) dh \quad (12)$$

In the limit of $R \to \infty$ Eq. 12 equals the common version of the Frumkin-Derjaguin equation.

Derivation of the Axial Stress in the Cylindrical Pore According to DBdB Theory

Within DBdB theory the grand potentials of adsorbed fluid in film and filled pore regime are given by [2]:

$$\Omega_{a,film}(p) = \Omega(0) - \int_{-\infty}^{\mu(p)} N_{a,film}(\mu')d\mu' \quad (S3a)$$

$$\Omega_{a,filled}(p) = \Omega(p_0) - \int_{0}^{\mu(p)} N_{a,filled}(\mu')d\mu' \quad (S3b)$$

Here the reference points are

$$\Omega(0) = 2\pi RL\gamma_s \quad (S4a)$$

$$\Omega(p_0) = 2\pi RL\gamma_{sl} - \pi R^2 L p_0 \quad (S4b)$$

To calculate the axial (tangential) stress $\sigma_{a,\parallel}$ we insert Eq. S3 and S4 into Eq. 5:

$$\sigma_{a,\parallel,film} = -\frac{\Omega_{a,film}}{V_p} = -\frac{2\gamma_s}{R} + \int_{-\infty}^{\mu(p)} \frac{N_{a,film}(\mu')}{V_p} d\mu' \quad (S5a)$$

$$\sigma_{a,\parallel,filled} = -\frac{\Omega_{a,filled}}{V_p} = -\frac{2\gamma_{sl}}{R} + p_0 + \int_{0}^{\mu(p)} \frac{N_{a,filled}(\mu')}{V_p} d\mu' \quad (S5b)$$

The solution of the integral in Eq. S5a is obtained by integration by parts:

$$\frac{1}{V_p}\int_{-\infty}^{\mu(p)} N_{a,film}(\mu')d\mu' = \frac{1}{V_p}\left[N_{a,film}(h') \cdot \mu(h')\right]_0^h - \frac{1}{V_p}\int_0^h \left[\mu(h') \cdot \frac{\partial N_{a,film}}{\partial h'}\right] dh' \quad (S6)$$

Inserting Eq. 6, 9a and $V_p = \pi R^2 L$ in Eq. S6 we get:

$$\begin{aligned}\frac{1}{\pi R^2 L}&\left[-V_L\left[\Pi(h') + \frac{\gamma_{lv}}{R-h'}\right] \cdot \frac{\pi L}{V_L}\left(2Rh' - h'^2\right)\right]_0^h \\ &- \frac{1}{\pi R^2 L}\int_0^h -V_L\left[\Pi(h') + \frac{\gamma_{lv}}{R-h'}\right] \cdot \frac{2\pi L}{V_L}(R-h')dh' \\ &= \frac{2}{R^2}\int_0^h (R-h')\Pi(h')dh' - \frac{h}{R}\left(2 - \frac{h}{R}\right)\Pi(h) - \frac{h^2}{R^2} \cdot \frac{\gamma_{lv}}{R-h} \quad (S7)\end{aligned}$$

Combining Eq. S5a and S7 results in Eq. 13a:

$$\sigma_{a,\parallel,film} = -\frac{2\gamma_s}{R} + \frac{2}{R^2}\int_0^h (R-h')\Pi(h')dh' - \frac{h}{R}\left(2 - \frac{h}{R}\right)\Pi(h) - \frac{h^2}{R^2} \cdot \frac{\gamma_{lv}}{R-h} \quad (13a)$$

Eq. S5b can be simplified by combination with Eq. 6 and 9b resulting in Eq. 13b:

$$\sigma_{a,\parallel,filled} = -\frac{2\gamma_{sl}}{R} + p_0 + \frac{R_g T}{V_L}\, ln\left({}^{p}/_{p_0}\right) \quad (13b)$$

Solution of the Lamé Problem for the Cylindrical Tube

When fluid is adsorbed inside the capillary tube, it exerts the adsorption stress on the inner wall and consequently causes strain within the tube. The resulting deformation is determined by the solution of the Lamé problem, here formulated in the cylindrical coordinates r, θ and z. The Lamé problem implies a system of equations for the radial, circumferential, and axial stresses $(\sigma_r, \sigma_\theta, \sigma_z)$ and respective strains $(\varepsilon_r, \varepsilon_\theta, \varepsilon_z)$. To simplify the situation we make several assumptions:

- Due to the axial symmetry of the capillary tube, all stresses and strains are independent of the angle θ.
- The adsorbate density distribution does not depend on the axial coordinate z. Consequently the same holds true for stresses and strains.
- The tube is sufficiently long ($L \gg R$) to assume, that the axial stress σ_z is also independent of the spatial coordinate r.

Based on these assumptions we obtain the following set of equations [3, 4]:

$$\varepsilon_r(r) = \frac{1}{E}\big(\sigma_r - \nu(\sigma_\theta + \sigma_z)\big) = \frac{du_r(r)}{dr} \quad (S8a)$$

$$\varepsilon_\theta(r) = \frac{1}{E}\big(\sigma_\theta - \nu(\sigma_r + \sigma_z)\big) = \frac{u_r(r)}{r} \quad (S8b)$$

$$\varepsilon_z = \frac{1}{E}\big(\sigma_z - \nu(\sigma_r + \sigma_\theta)\big) = \frac{du_z(z)}{dz} = const. \quad (S8c)$$

Here, $u_r(r)$ is the radial and $u_z(z)$ is the axial displacement within the cylindrical tube. E and ν are the Young modulus and Poisson ratio of the solid, respectively. The sought strains are the axial strain $\varepsilon_z = \delta L/L$ and the circumferential strain at the outer surface of the capillary, $\varepsilon_\theta(R_{out}) = \delta R_{out}/R_{out}$, determining the change of the tube size in the radial direction.

From the balance of the axial adsorption stress exerted by the fluid and the axial stress in the solid tube it follows that

$$\sigma_z = \frac{\phi}{1-\phi}\sigma_{a,\parallel} \quad (S9)$$

For the axial and circumferential stresses we assume the form of $\sigma_r = A + B/r^2$ and $\sigma_\theta = A - B/r^2$, respectively, complemented by the boundary conditions $\sigma_r(r = R) = \sigma_{a,\perp}$ and $\sigma_r(r = R_{out}) = 0$ [4]. This approach leads to $A = \phi/(1-\phi)\sigma_{a,\perp}$ and $B = -Aa^2$ resulting in

$$\sigma_r = \frac{\phi}{1-\phi}\left(1 - \frac{R_{out}^2}{r^2}\right)\sigma_{a,\perp} \quad (S10a)$$

$$\sigma_\theta = \frac{\phi}{1-\phi}\left(1 + \frac{R_{out}^2}{r^2}\right)\sigma_{a,\perp} \quad (S10b)$$

with the important consequence that

$$\sigma_r + \sigma_\theta = \frac{2\phi}{1-\phi}\sigma_{a,\perp} = \sigma_\theta(R_{out}) = const. \quad (S11)$$

Inserting Eq. S9, S10 and S11 into Eq. S8 the following equations are held for the strains:

$$\varepsilon_r(R_{out}) = -\frac{\nu}{E}\frac{\phi}{1-\phi}(2\sigma_{a,\perp} + \sigma_{a,\parallel}) \quad (S12a)$$

$$\varepsilon_\theta(R_{out}) = \frac{1}{E}\frac{\phi}{1-\phi}(2\sigma_{a,\perp} - \nu\sigma_{a,\parallel}) \quad (S12b)$$

$$\varepsilon_z = \frac{1}{E}\frac{\phi}{1-\phi}(\sigma_{a,\parallel} - 2\nu\sigma_{a,\perp}) \quad (S12c)$$

Eq. S12b and S12c correspond to Eq. 14 and 15.

Determination of the Reference Isotherm for DBdB Theory

For the determination of the disjoining pressure $\Pi(h)$ on sintered silica we prepared a purely macroporous reference sample. The reference sample was synthesized following the same protocols as the sample prepared for the in-situ dilatometry experiment [5, 6], but dried in an autoclave using supercritical CO_2 and subsequently calcined/sintered at 1000 °C for 20 min in ambient atmosphere. The bulk density of the monolithic sample ρ = (0.647 ± 0.038) g/cm³ was determined after degassing at 110 °C for 1 d at gas pressures below 10^{-3} mbar. The lack of micro- and mesopores was validated by scanning electron microscopy (Figure S1) and N_2 adsorption at 77 K (Figure S2). From the N_2 adsorption isotherm we derived the BET-surface area S_{BET} = (9.9 ± 0.5) m²/g [7], the disjoining pressure Π and the average film thickness h by [8]

$$\Pi = -\frac{R_g T}{V_L} ln\left({}^{p}/_{p_0}\right) \quad (S13)$$

$$h = \frac{N_a \cdot V_L}{m_{sample} \cdot S_{BET}} \quad (S14)$$

Here R_g is the gas constant and V_L = 34.66 cm³/mol the molar liquid volume of liquid nitrogen at the temperature of T = 77.4 K. The resulting $\Pi(h)$ correlation is shown in Figure S3 along with an empirical fit (see e.g. [8])

$$\Pi(h) = \Pi_1 \, exp\left(-\frac{h}{\lambda_1}\right) + \Pi_2 \, exp\left(-\frac{h}{\lambda_2}\right) \quad (S15)$$

The respective parameters applied were Π_1 = 178 MPa, λ_1 = 0.23 nm, Π_2 = 68 MPa and λ_2 = 0.073 nm. The reference isotherm resulting from the combination of Eq. 6 (in the limit of $R \to \infty$) and S15 is also shown in Figure S2.

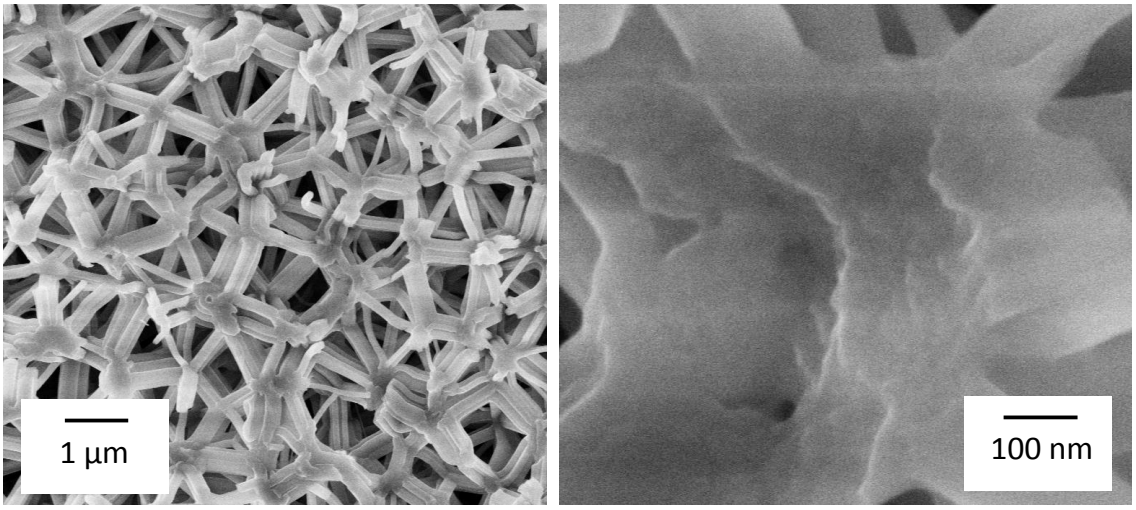

Figure S1. SEM images of the reference sample.

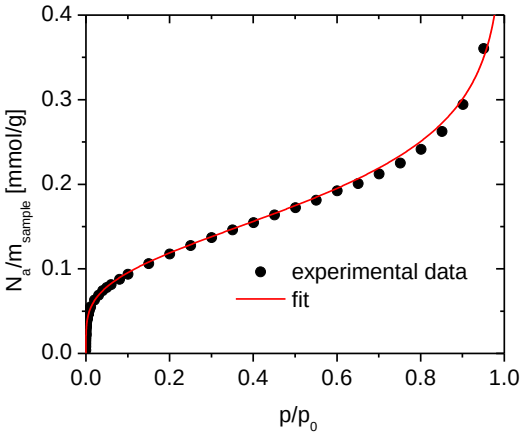

Figure S2. N_2 adsorption isotherm of the reference sample and respective reference isotherm according to the combination of Eq. 6 and S15.

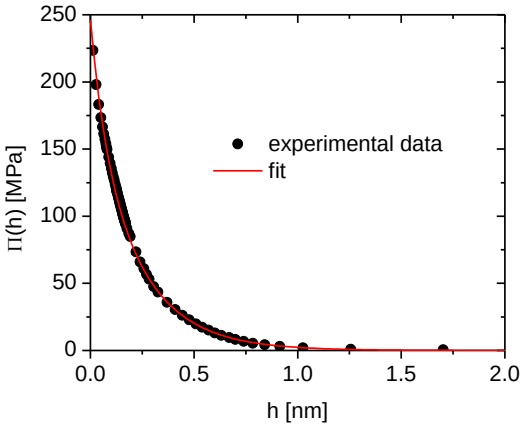

Figure S3. Disjoining pressure $\Pi(h)$ derived from the experimental N_2 adsorption isotherm and respective fit according to Eq. S15.

Dependence of Axial and Circumferential Strain on the Poisson's Ratio

To investigate the impact of the nonporous backbone's Poisson's ratio on the theoretical strains we calculated the axial and radial stresses, $\varepsilon_{a,\perp}$and $\varepsilon_{a,\parallel}$, according to Eq. 10 and 13, respectively, for ν = 0.15, 0.2 and 0.25 (see Figure S4). This covers the full range of reasonable values for ν. Since the Young's modulus E of the nonporous backbone is a simple scaling factor for the strains, we plotted strain multiplied by E in Figure S4. As can be seen from Figure S4, the variation of ν does not change the shape of the strain isotherm, but results essentially in a scaling of $\varepsilon_{a,\perp}$and $\varepsilon_{a,\parallel}$ similar to the Young's modulus, i.e. smaller values of ν lead to larger strains and vice versa. The overall variation of $\varepsilon_{a,\perp}$and $\varepsilon_{a,\parallel}$ for different values of ν is rather small though.

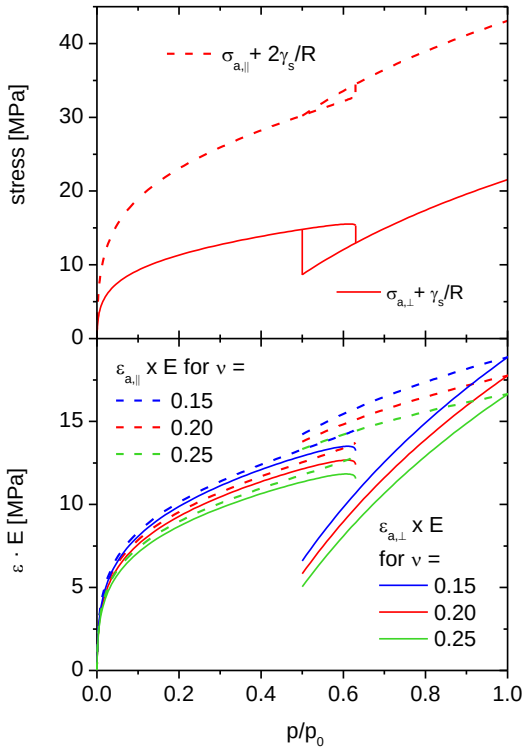

Figure S4. Upper panel: axial and radial stresses derived by Eq. 10 and 13 set to zero stress at vacuum conditions. Lower panel: axial and radial strains derived from the stresses in the upper panel for the cylindrical tube model (Eq. 14 and 15) multiplied by the Young's modulus E. The Poisson ratio of the nonporous solid backbone was set to ν = 0.15, 0.2 and 0.25.

Prediction of Strain Isotherm from in-situ Scattering

Figure S5 shows a comparison of the experimental strain isotherm obtained for the model system via in-situ dilatometry and the respective modeling by the proposed theoretical framework (Eq. 20) as presented in Figure 8. Additionally, the prediction for the circumferential strain $\varepsilon_{a,\perp}$ (Eq. 14) corresponding to a hypothetical strain isotherm from in-situ scattering is included. All model parameters applied for the prediction of $\varepsilon_{a,\perp}$ are identical to the modeling of the in-situ dilatometry data. As can be seen from Figure S5, $\varepsilon_{a,\perp}$ exhibits a pronounced triangular behavior in the region of

capillary hysteresis that is typical for most of reported experimental data obtained by in-situ scattering on mesoporous materials, e.g. [9, 10]. As expected, it is drastically different from the dilatometrically measured strain in the hysteresis region due to the anisotropic geometry of pore channels.

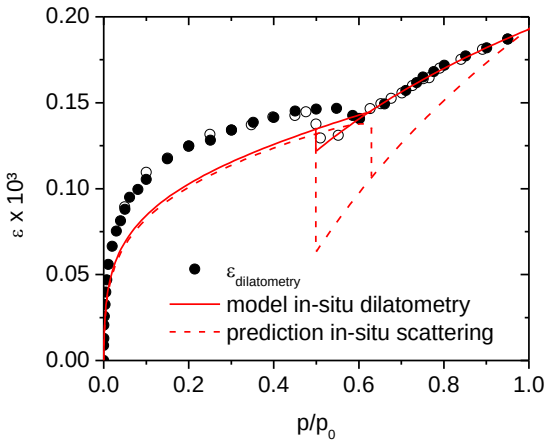

Figure S5. Strain isotherm obtained by in-situ dilatometry for the model system complemented by the theoretical strain isotherms for in-situ dilatometry (Eq. 20) and the in-situ scattering (Eq. 14).

References

[1] T.L. Hill, Theory of Physical Adsorption, Advances in Catalysis 4 (1952) 211-258.
[2] G.Y. Gor, A.V. Neimark, Adsorption-Induced Deformation of Mesoporous Solids, Langmuir 26 (2010) 13021-13027.
[3] T.M. Atanackovic, A. Guran, Theory Of Elasticity For Scientists and Engineers, Birkhäuser, Bosten, 2000.
[4] S. Timoshenko, J.N. Goodier, Theory of Elasticity, McGraw-Hill Book Company, New York, 1951.
[5] D. Brandhuber, N. Huesing, C.K. Raab, V. Torma, H. Peterlik, Cellular mesoscopically organized silica monoliths with tailored surface chemistry by one-step drying/extraction/surface modification processes, Journal of Materials Chemistry 15 (2005) 1801-1806.
[6] D. Brandhuber, V. Torma, C. Raab, H. Peterlik, A. Kulak, N. Husing, Glycol-modified silanes in the synthesis of mesoscopically organized silica monoliths with hierarchical porosity, Chemistry of Materials 17 (2005) 4262-4271.
[7] S. Brunauer, P.H. Emmett, E. Teller, Adsorption of Gases in Multimolecular Layers, Journal of the American Chemical Society 60 (1938) 309-319.
[8] G.Y. Gor, O. Paris, J. Prass, P.A. Russo, M.M. Ribeiro Carrott, A.V. Neimark, Adsorption of n-pentane on mesoporous silica and adsorbent deformation, Langmuir 29 (2013) 8601-8608.
[9] G. Dolino, D. Bellet, C. Faivre, Adsorption strains in porous silicon, Physical Review B 54 (1996) 17919-17929.
[10] G. Günther, J. Prass, O. Paris, M. Schoen, Novel Insights into Nanopore Deformation Caused by Capillary Condensation, Physical Review Letters 101 (2008) 086104.